Tanzania Journal of Science 49(3): 677-689, 2023
ISSN 0856-1761, e-ISSN 2507-7961

Hydro-geochemistry and Related Processes Controlling the Composition of Thermal Waters in the Lake Natron Basin, Northern Tanzania

Edista A. Abdallah[1]*, Charles H. Kasanzu[1], Crispin P. Kinabo[1] and Akira Imai[2]
[1]Department of Geosciences, University of Dar es Salaam, P.O. Box 35052, Dar es Salaam, Tanzania.
[2]Department of Earth Resources Engineering, Kyushu University, Japan.
Email addresses; abdister@udsm.ac.tz; kcharls16@yahoo.com; kinabo_2003@yahoo.co.uk; imai@mine.kyushu-u.ac.jp*
**Corresponding author*
Received 14 Apr 2023, Revised 22 Aug 2023, Accepted 22 Aug 2023 Published Sep 2023
DOI: https://dx.doi.org/10.4314/tjs.v49i3.11

Abstract

Lake Natron Basin (LNB) forms part of the eastern branch of the East African Rift System (EARS) in Tanzania. The basin is endowed with thermal springs flowing towards the lake from the western, northwestern, southwestern and eastern parts. The western, northwestern and south-western thermal springs emanate from fractures in the basaltic rocks while in the east, they originate from the western flank of the Gelai volcano. There are limited studies on these springs, thus their geochemical differences and distributions of physicochemical parameters are not well understood. A hydrogeochemical study was conducted to interpret available geochemical data from the LNB springs, including cold and thermal water to allow their geochemical characterization. Results have shown that LNB water is dominated by sodium (Na^+), chloride (Cl^-) and bicarbonate (HCO_3^-) ions. Three hydro-chemical facies have been identified forming Na-Cl, Na-HCO_3 and Ca-HCO_3 water types. This study has also revealed that thermal water in the north-western part of the basin is highly mineralised and gradually becomes diluted toward south-west and south due to groundwater incursion. Water-CO_2-rock interaction affects the overall chemistry of thermal water leading to HCO_3^- water, particularly in the east of the basin. While few springs from the western side of the basin indicated maturity of the thermal waters, other springs indicated mixed Cl-HCO_3/peripheral water; while the cold waters are HCO_3 type. It is recommended to take precautions when planning geothermal projects to avoid corrosion and scaling of production facilities. Similarly, mixing or dilution of thermal water with shallow groundwater can affect the temperature and the composition of Cl^-.

Keywords: thermal water, Lake Natron Basin, thermal springs, hydro-geochemistry.

Introduction

Geochemistry is an important tool for geothermal investigation, as it is based on the variation in distribution of chemical solutes in the geothermal fluids (D'Amore and Panichi 1985). Hydrothermal fluids contain reactive constituents (e.g. Na, K, Mg and Ca) and non-reactive constituents (e.g. Cl and boron (B)). These constituents take part in temperature-dependent chemical reactions and therefore provide support on temperature estimation and serve as indicators of geochemical processes including water-rock interaction, surface evaporation, mixing and dilution with fluids of different origins (Giggenbach 1988, Tian et al. 2018).

Lake Natron Basin (LNB) is one amongst a series of enclosed sedimentary basins of the eastern branch of the East African Rift System (EARS) in Tanzania (Dawson 2008).

It is well known for its abundant hydrothermal activities. Due to the active rifting and volcanism, the basin is endowed with thermal springs flowing towards the lake from the western, north-western, south-western and eastern parts. The western, north-western and south-western thermal springs emanate from fractures in the basaltic rocks while in the east, they originate from the western flank of the Gelai volcano feeding the eastern part of the lake (Mahecha et al. 2018).

The earliest study of LNB thermal springs was conducted by Guest and Steven (1951) who attempted to account for the geochemical composition of Lake Natron springs and brines. Eugster (1970) interpreted the presence of springs with high temperatures exceeding 50 °C on the western side, as an evidence of a deep-seated heat source. It was reported that other parameters such as Cl^- are higher on the NW part of the basin and lower on the SW side of the lake (Eugster 1970). Furthermore, the thermal springs of the East Lake Natron Basin (ELNB) indicated a poor Cl^- trend and showed no steadiness in Na/Cl content. While there were no HCO_3^- measurements, the report showed a regional variation in the SO_4^{2-}/Cl^- ratios, where the lowest ratios were found in the NW (i.e., in chloride-rich springs) and increased gradually towards the south. The highest SO_4 occurs in the SW which is considered to be a result of mixing (Eugster 1970).

Lake Natron hydrothermal system was mapped and classified as an advective brine system of low temperature occurring in an arid climatic region discharging along the rift wall (Hochstein 1999, Hochstein et al. 2000). Hochstein et al. (2000) suggested that the brine discharged by the spring evaporates and forms crystalline carbonates of sodium (trona) on the Rift Valley floor. As Hochstein et al. (2000) postulated, heat from the upper crustal rocks is swept by water infiltrating the higher rift shoulders, attaining in part their mineral content by leaching of the surrounding sediments. The crustal CO_2 flux enhances the development of the bicarbonate brines (Hochstein et al. 2000). Muirhead et al. (2016) used the geochemistry of thermal springs to investigate the role of magmatic volatile release in the rift basin evolution. It has been reported that there is a strong relationship between the evolution of the upper crust strain and the release of fluids from deep magma bodies in the EARS. Likewise, Lee et al. (2017) used geochemistry and isotopes of volatiles from the hydrothermal systems to constrain the sources and fluxes of volatiles in the basin. The volatiles are reported to have originated from the mantle and the upper crust (Lee et al. 2017). Recently, Mahecha et al. (2018) noted the differences in surface temperature of thermal springs in the LNB suggesting that the ELNB temperatures are lower than those in the West Lake Natron Basin (WLNB).

While earlier reports provide information about the LNB, some of the reported data are old and could not provide detailed geochemistry of the area (Guest and Stevens 1951, Eugster 1970). Subsequent researchers in the LNB relied on these insufficient data; therefore, updated geochemical data are vital for an improved understanding of different geochemical signatures. This study focused on detailed investigation and interpretation of hydrogeochemical data of cold and thermal water from the springs in Lake Natron Basin (LNB). Special emphasis is on the characterisation of thermal waters in terms of geochemical evolution and compositions; to assess and classify the hydrothermal systems in the LNB in terms of maturity; and to evaluate the mixing or dilution between thermal waters and other sources in the LNB.

Geological settings

The study area is located at Lake Natron Basin (LNB) in northern Tanzania within the geographic limit of longitude 35°50' to 36°10' E and latitude 2°40' to 2° 00' S. It is bounded in the west by the Natron Boundary Fault of the EARS and in the east by the extinct shield volcano, the Gelai and undulating hills towards the north to the Kenyan border. In the south occurs Oldoinyo Lengai active volcano formed of tuffs and agglomerates with flows of nephelinites, phonolite and

natrocarbonatite (Dawson 2008, Muirhead et al. 2016).

The LNB is marked by diversified geology and complex geological structures (Figure 1). The geology is made of volcanic features that vary dramatically in age, composition and size, ranging from late Miocene and Pliocene shield volcanoes e.g. Gelai to younger intermediate composite and carbonatite volcanoes e.g. Oldoinyo Lengai (Dawson 2008). The dominant rocks in the area are olivine basalts, trachytes and phonolites that are associated with the Neogene volcanoes, quartzo-feldspathic gneisses that make up the basement rocks and Pleistocene to Recent sediments (Dawson 2008, Neukirchen et al. 2010).

Plio-Pleistocene lacustrine sediments of the Peninj Group are exposed in the uplifted footwall of the Lake Natron boundary fault system across the Salei Plain (Figure 1). They are composed of conglomerates, sands and clays interbedded with tuff, formed by sediments of the Moiniki River valley and Salei Plain. The sediments are unconformably overlying the basaltic sequences in the west of Lake Natron (Foster et al. 1997). Recent sediments are characterized by natural salts of Lake Natron (trona) and black volcanic ashes ejected from Oldoinyo Lengai (Foster et al. 1997, Dawson 2008).

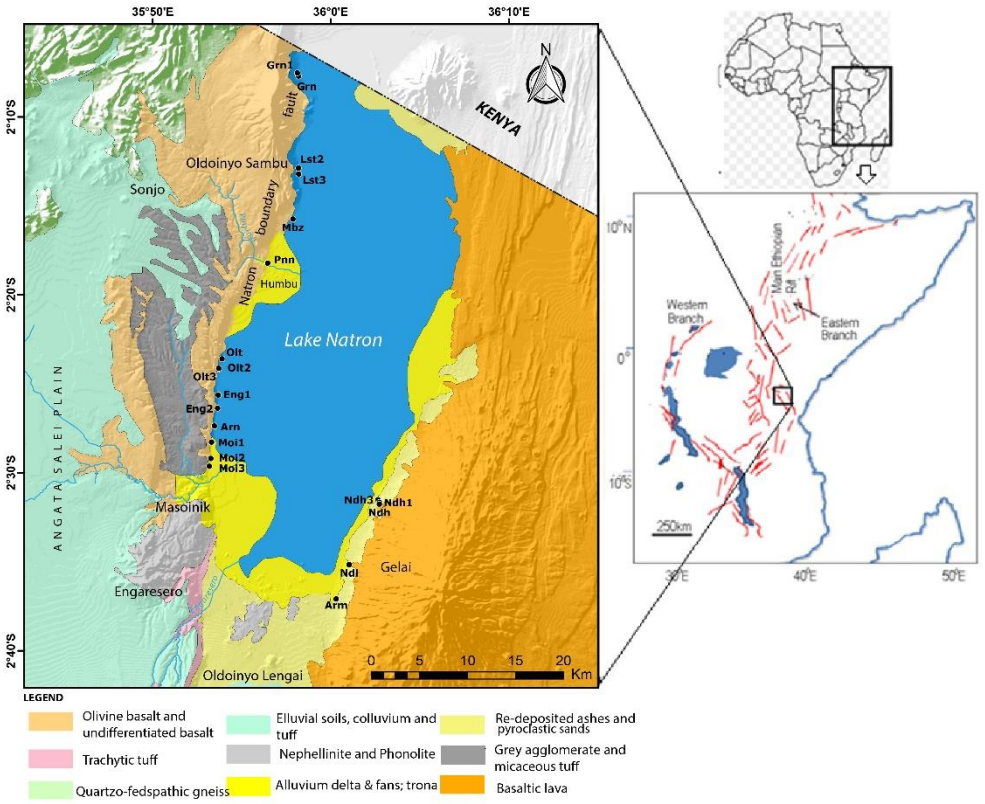

Figure 1: Map showing a summarised geology of Lake Natron Basin in Northern Tanzania (Modified after Guest et al. 1961, Guest and Pickering 1966a, Guest and Pickering 1966b, Abdallah et al. 2022). Lst = Lesiteti, Grn = Gerileni Mbz = Mbazi, Pnn = Pinyinyi, Olt = Olajata, Eng = Engong'owasi, Arn = Arng'arwa, Moi = Moiniki, Arm = Armaniti, Ndl = Ndalesindai and Ndh = Ndahane.

The salt crust consists mainly of sodium carbonate (trona) and common salts. The area covered by these evaporites varies both with the season and the year (Dawson 2008).

Materials and Methods

Sampling and analysis

Twenty-three (23) water samples were collected from thermal and cold springs; and rivers in the LNB between January and December 2021. Data collection and analysis of chemical parameters followed the procedures described by Nicholson (1993) and Arnórsson et al. (2006). The water samples were collected at the spring's outlet and were stored in high-density polyethylene bottles. Temperature (T), electrical conductivity (EC) and pH were measured *in situ* using YSI professional plus multi-parameter instrument before the collection of samples. The instrument was calibrated in accordance with the manufacturer's recommendation. Two labelled plastic bottles of 1 litre each were used for collection of water samples. The sample from one of the bottles was filtered through the 0.45 µm pore size filters, and then stored in a 100 ml pre-acidified (ultrapure HNO_3) high-density polyethylene bottle, for major cation analyses. Acidification was carried out to prevent the cation contents of higher temperatures from becoming supersaturated upon cooling (Davraz 2014). 200 ml of filtered, un-acidified water sample was added into a polyethylene bottle for the determination of anions. The second 1 litre untreated water sample bottle was kept for anion analysis in the laboratory.

Alkalinity, chloride, fluoride and nitrate analyses were performed at the Department of Geosciences of the University of Dar es Salaam in Tanzania. Alkalinity was measured by volumetric titration against 0.1600 N H_2SO_4 using bromocresol green-methyl indicator by Hach® titration kits. Similarly, chloride (Cl^-) was measured by the $HgNO_3$ method by Hach® titration kits, whereas sulphate (SO_4^{2-}) and nitrate (NO_3^-) were determined by using a spectrophotometer (Hach®, DR/3900) and fluoride (F^-) was determined using Hach® DR/2400.

Major cation and trace element analysis was conducted at the ICP-MS Laboratory University of Stellenbosch in South Africa. Data was quantified with calibration solutions prepared from NIST traceable standards, and quality control procedures according to US EPA guidelines to ensure the accuracy of the produced data. The quality of water analysis was subjected to ionic balance calculation (equation 1) as explained by Appelo and Postma (2005).

$$\text{Electrical Balance (EB)}\% = \left(\frac{\Sigma\text{cation} + \Sigma\text{anion}}{\Sigma\text{cation} - \Sigma\text{anion}}\right) x\ 100 \qquad (1)$$

Whereby the contributions to charge are in units of meq/l. The charge balance error for chemical analysis was within the acceptable range of (±5 %). Golden Software Grapher 14, and Geochemical Plotting Spreadsheet by Powell and Cumming (2010) were used for data analyses and interpretation. Powell and Cumming (2010) Geochemical Plotting Spreadsheet uses formulas that are based on equilibrium reactions and empirical relationships to generate cross-plots and ternary diagrams for analysing and interpreting thermal water samples. Geochemical classification of water was performed by using the Piper (1944) diagram and CL-SO_4-HCO_3 water classification scheme of Giggenbach (1991).

Results

Characteristics of thermal springs

A summary of sample locations and geochemical results is listed in Table 1. The discharge temperature of the thermal waters in the Western Lake Natron Basin (WLNB) varied from 34 °C in Arng'arwa (Arn) to 51.2 °C Olajata (Olt1) with a mean value of 40.4 °C while the pH values varied from 9.1 in Mbazi (Mbz) to 10.7 in Lesitate (Lst 2 & Lst3) with a mean value of 9.9. The electrical conductivity (EC) of thermal waters varied from 5007 µs/cm Engong'owasi (Eng2) to 49200 µs/cm in Gerleni (Grn) having a mean value of 21369 µs/cm. The pH of cold waters in the WLNB ranged between 7 in Pinyinyi (Pnn) and 8.9 (Moi2) with a mean value of 8, while the EC ranged from 284 µs/cm (Pnn) to

3806 µs/cm (Moi2) with a mean value of 1652 µs/cm. The alkalinity of thermal water ranged from 350 mg/l (Eng2) to 8380 mg/l (Grn1), while that of cold water ranged from 130 mg/l in Pnn river to 450 mg/l Moi2 spring.

In East Lake Natron Basin (ELNB), the pH of thermal water indicated neutral to near neutral characters ranged between 7.7 in Ndahane (Ndh3) and 8.8 in Ndalesindai (Ndl). The temperature ranged from 35.7 °C in Ndl to 43.7 °C in Ndh3. The EC ranged between 5075 µS/cm in Arm and 17510 µS/cm in Ndh3, while the alkalinity was between 1890 mg/l (Arm) and 6280 mg/l (Ndh3). Given that majority of samples had a pH range from near neutral to a maximum of 10.7, bicarbonate (HCO_3^-) was assumed to be a dominant constituent of alkalinity.

Major cations in the WLNB were in the order of $Na^+ > K^+ > Ca^{2+} > Mg^{2+}$. The dominant cation was sodium (Na^+) with the highest value of 11530 mg/l measured at Grn and the lowest was 1159 mg/l, at Eng2 with a mean value of 4177 mg/l, followed by potassium (K^+) with the highest value of 170.5 mg/l at Grn1 and the lowest 31.0 mg/l at Eng2 with a mean value of 70 mg/l. Calcium (Ca^{2+}) was between 0.39 mg/l and 1.37 mg/l with a mean value of 0.6 mg/l, while magnesium (Mg^{2+}) was little or below the detection limit in some samples. The major anions were in the order of $Cl^- > HCO_3^- > SO_4^{2-}$ dominated by chloride (Cl^-) where the highest value was 9539 mg/l measured at Grn and the lowest was 1715 mg/l at Eng2 with a mean value of 4420 mg/l. The highest value of SO_4^{2-} was 150 mg/l measured at Grn1 and the lowest was 1 mg/l measured at Mbz and Lst2. Cold water behaved differently in terms of major ions, the dominant cation was Na^+ except for Pnn river, in which calcium (Ca^{2+} = 28 mg/l) was dominant while bicarbonate (HCO_3^- = 108 mg/l) was a dominant anion. The Moiniki cold water was dominated by Na^+ ranging from 18 mg/l to 778 mg/l with a mean value of 21 mg/l. In contrast, anions in Moi1 and Moi3 were dominated by HCO_3^- =310 mg/l except for Moi2 in which the dominant anion was chloride ($Cl^- > HCO_3^-$).

In the ELNB major cations were in the order of $Na^+ > K^+ > Mg^{2+}$ with Na^+ dominating and anions were in the order of $HCO_3^- > Cl^- > SO_4^{2+}$ with HCO_3^- and Cl^- being the most abundant. The Na^+ concentrations were in the range of 1384 mg/l (Arm) and 4327 mg/l (Ndh3) with a mean of 2459 mg/l. The K^+, Mg^{2+}, and Ca^{2+} concentrations were in the range of 29.1 mg/l (Arm) to 107.4 mg/l (Ndh3) with a mean of 56.1 mg/l for K^+, 0.5 mg/l (Ndh3) to 4.0 mg/l (Arm) with a mean of 1.4 mg/l for Mg^{2+}, and 0.4 mg/l (Ndh3) to 1.06 mg/l (Arm) with a mean of 0.57 mg/l for Ca^{2+}. The concentrations of HCO_3^- were in the range of 1890 mg/l (Arm) and 6280 mg/l (Ndh3) with a mean of 3350 mg/l. The Cl^-, NO_3^- and SO_4^{2-} were in the range of 1180 mg/l (Arm) to 2953 mg/l (Ndh3), 5 mg/l (Ndh2) to 13.6 mg/l (Ndh1), 2 mg/l (Ndh2) to 18 mg/l (Arm) with mean values of 1918.6 mg/l, 10.0 mg/l and 6.8 mg/l, respectively.

Table 1: Descriptive statistics (minimum, maximum, mean and standard deviation) of the physicochemical parameters of thermal and cold waters of LNB

	Elevation m	Temp °C	pH	EC µS/cm	SO_4^{2-} mg/l	NO_3^- mg/l	Cl^- mg/l	HCO_3^- mg/l	F^- mg/l	Ca^{2+} mg/l	K^+ mg/l	Mg^{2+} mg/l	Na^+ mg/l	B^{3+} mg/l
West Lake Natron														
Min	602	34.0	9.1	5007	1.0	2.1	1714	350	1.87	0.3	<1.0	3.4	1159	0.1
Max	612	51.2	10.7	49200	150	17.5	9538	8380	5.8	1.3	170.5	3.4	11530	12.9
Mean	608	40.4	9.9	21369	44.8	12.2	4420	2829	3.6	0.6	70	3.4	4177	4.6
SD	3.7	5.0	0.5	12330	46	4.1	2367	2495	2.0	0.2	47	NA	2877	3.7
East Lake Natron														
Min	603	34.4	7.7	5075	2.0	5.0	1179.7	1890	1.6	0.3	29.1	0.4	1384	0.0
Max	630	43.7	8.8	17510	18	13.6	2952.7	6280	3.3	1.0	107.4	4.0	4327	0.6
Mean	617.5	38.0	8.2	9859	6.8	10.0	1918.6	3350	2.2	0.5	56.0	1.4	2459	0.2
SD	9.3	3.2	0.5	4154	5.9	3.6	616.7	1545	0.9	0.2	27.6	1.3	1014	0.3
Cold water														
Min	607	28.3	7.0	284	12	0.2	8.1	139	0.4	0.2	1.3	0	18	0.9
Max	633	32.5	8.9	3806	150	4.4	851.7	450	2.6	28	19	7.4	775	2.9
Mean	620.2	30.9	8.0	1652	87	1.8	297.3	334	1.5	7.3	7.0	2.6	21	1.6
SD	11.2	1.8	0.8	1511	56	1.8	390	145	1.6	13.7	8.4	4.1	375	0.7

Discussion

Geochemical characteristics

The geochemical evolution of thermal and cold water involves several factors including the source of recharge, flow path, mixing and water-rock interaction processes (Wang et al. 2018). These in turn provide the geochemical characteristics of the hydrothermal system detected in the thermal and cold water from the springs. The physicochemical parameters measured in the WLNB show a decreasing trend towards the south of the basin (Figure 2). For example, the EC was higher in the NW of the basin (up to 49,000 µS/cm) than in the SW, reflecting more dissolved constituents, as thermal water interacts thermodynamically with the lithology in the study area. However, in the SW, this parameter decreased. This has probably resulted from mixing/dilution with cold water from the Pinyinyi River (EC = 284 µS/cm) and/or from groundwater encroaching on the nearby thermal springs (e.g., Eugster 1970, Petrini et al. 2013). These values continue to be high (greater than 1000 µS/cm) in ELNB but are lower than WLNB values due to high levels of water-rock interactions that are enhanced by secondary permeability (Muirhead et al. 2016, Abdallah et al. 2022).

The pH of thermal water in the WLNB ranged between 8.3 and 10.7 indicating basic properties. The alkaline property is caused by CO_2 flux which affects thermal water by changing the pH (e.g. Lee et al. 2017). Nicholson (1993) proposed that the brines and the loss of CO_2 upon boiling make the solution progressively more alkaline. The pH in the ELNB thermal water is nearly equal to the cold waters of the study area (pH = 7 to 8.8). Nevertheless, the surface temperature of thermal water in the ELNB is lower than that of WLNB (e.g. Mahecha et al. 2018). For instance, Ndahane thermal spring in the ELNB measures the highest surface temperature (T = 43.7 °C) which is lower than Olajata thermal spring in WLNB (T = 52.2 °C).

This lowering of the temperature and the pH of thermal springs in the ELNB is caused by the dilution or mixing of thermal water with shallow groundwater. Like in the WLNB, the dominant cation in the ELNB was Na^+ and the dominant anions were HCO_3^- and Cl^-. High HCO_3^- concentrations were observed in the ELNB, which could be a result of water-CO_2-rock interaction as demonstrated by the HCO_3-rich thermal springs and carbonate-altered rocks as reported in Abdallah et al. (2022).

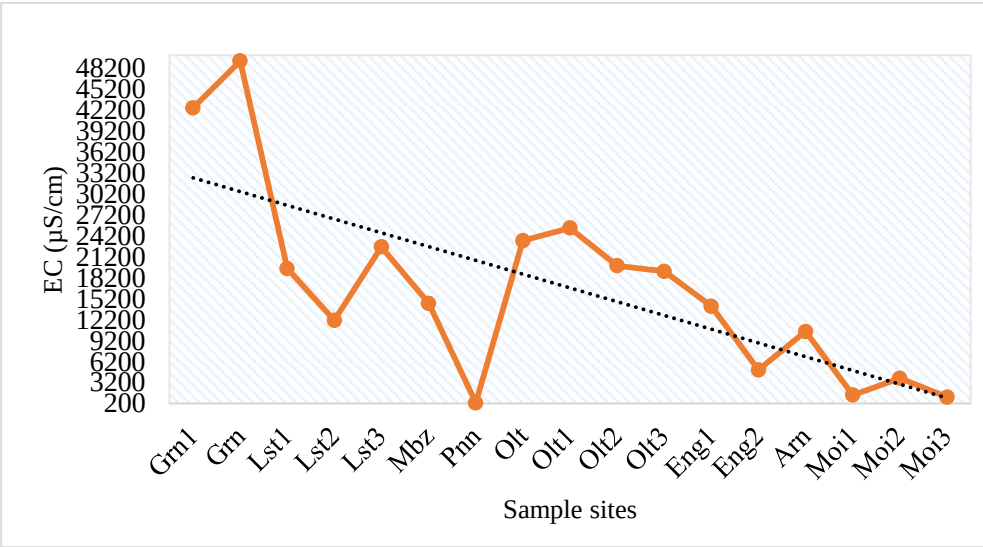

Figure 2: A diagram of the variation of EC (µS/cm) in the WLNB as indicated by the orange (solid) line.

Nicholson (1993) and Tian et al. (2018) have shown that the concentrations of SO_4^{2-} increase with the increase of oxidation of sulphide minerals and dissolution of gypsum. In LNB cold water, high SO_4^{2-} concentrations are due to steam condensation into near-surface water. The SO_4^{2-} concentrations ranged from 1 mg/l to 150 mg/l where the maximum value was measured at the southwest of the basin suggesting dilution between thermal water, surface water and shallow groundwater (e.g. Eugster 1970). Low to medium NO_3^- concentrations ranging between 2.1 mg/l and 17.5 mg/l in the WLNB and 5 mg/l and 13.6 mg/l in the ELNB are mostly caused by domestic animals and a minor contribution from agricultural activities in the study area. The high B^{3+} concentration of up to 12.9 mg/l is attributed to thermal fluids and intensive interaction between water and rocks especially in the WLNB.

Classification of thermal waters in LNB

To understand the geochemical evolution of thermal water, the concentrations of major ions were plotted on the Piper (1944) trilinear diagram which is based on the relative amounts of Na^+, K^+, Mg^{2+}, Ca^{2+}, Cl^-, SO_4^{2-}, and $HCO_3^- + CO_3^{2-}$ in a fluid (Figure 3). The LNB waters distinguished four water types; sodium-chloride (Na-Cl) and sodium bicarbonate (Na-HCO_3) for thermal water and calcium bicarbonate (Ca-HCO_3) and Na-HCO_3 for cold water.

Sodium was a dominant cation while Cl^- and HCO_3^- were the main anionic constituents in both thermal and cold water of LNB, forming Na-Cl and Na-HCO_3 water types. The Na-Cl water type occurred in almost all the thermal springs in the WLNB except Moiniki thermal spring. The high Na^+ concentration in the LNB thermal water resulted from ion exchange process involving Na/K-silicates from the reservoir rocks such as albite and K-feldspar (Lambrakis et al. 2014).

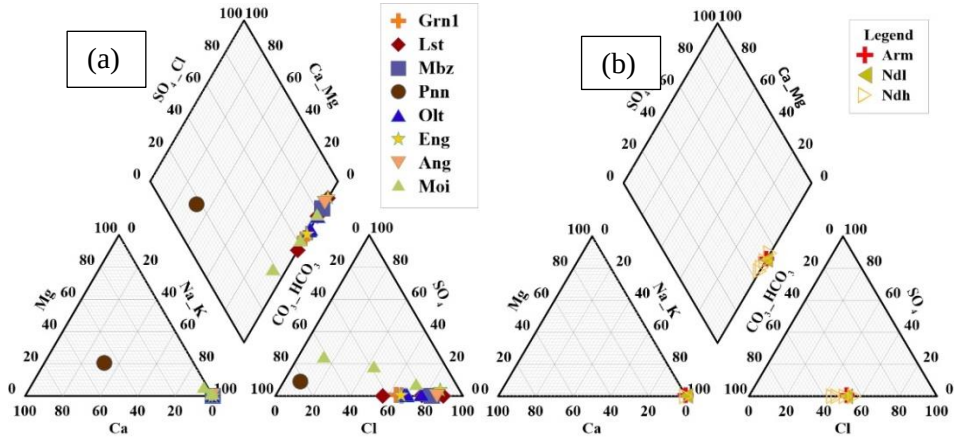

Figure 3: Piper diagrams for the samples analysed for major ion chemistry. Figure (a) represents WLNB samples while figure (b) is the ELNB samples.

Additionally, long periods of interactions between water and its host rocks, as well as mixing with water from other sources are responsible for the chemistry of thermal water of the LNB (e.g. Abdallah et al. 2022). Evaporation occurs at a high rate resulting in the formation of brines and precipitation and dissolution of minerals both affecting the water composition.

LNB is characterised by the release of mantle CO_2 related to the carbonatitic volcano of Oldoinyo Lengai through the soils and thermal springs. The gas contributes to the formation of HCO_3^- as a product of primary hydrolysis of silicate minerals from the reservoir rock leading to Na-HCO_3 water as interactions with rocks occur (e.g. Nicholson 1993, Tian et al. 2018). Jones et al.

(1977) and Li et al. (2021) have shown that silicate minerals and glasses of pyroclastic material hydrolyse rapidly in the rift areas, producing bicarbonate-rich waters. The Pinyinyi River water is Ca-HCO_3 type due to the short residence time that could not allow interactions with surrounding rocks. It is likely, that the water of the Pinyinyi River originates from rain and groundwater seepage.

Cl-SO_4-HCO_3 thermal water classification diagram

The Cl-SO_4-HCO_3 ternary diagram by Giggenbach (1991), indicated that Cl-CO_3 chemical facies occur both west and east of the basin (Figure 4). Three types of water were identified; HCO_3 water, mature Cl water and dilute Cl-HCO_3/peripheral water. The HCO_3 water type is represented by samples (Moi1, Moi3 and Pnn). This water has suffered little or no interaction with the host rocks due to the short residence time in the hydrothermal system and is likely to have originated from the shallow, cooler reservoir. The water has a high HCO_3^- concentration and low EC values (284 µS/cm-3806 µS/cm).

Except for the water from Grn1, Grn, Olt3 and Eng2, the thermal waters of WLNB are categorised as mature Cl water typical of the deep geothermal fluids found in high-temperature geothermal systems (Giggenbach 1988, Nicholson 1993). The mature Cl water emerges to the surface with minimum contamination with groundwater and is in equilibrium with reservoir rocks near the surface (Giggenbach 1988). The composition may be an indication that water has suffered a significant amount of evaporation, although the topography of an area may also play a significant role (D'Amore and Panichi 1985, Nicholson 1993).

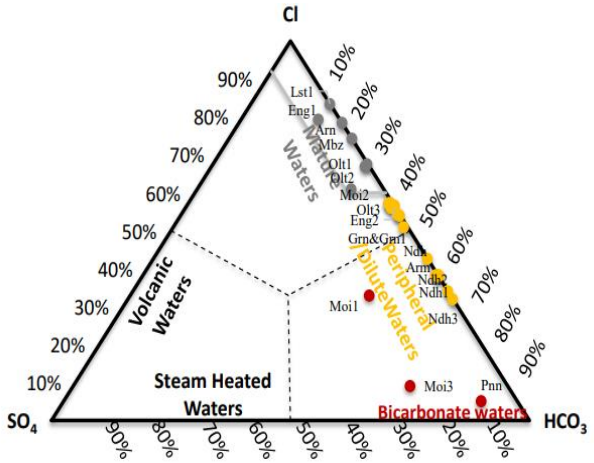

Figure 4: Ternary plot classifying thermal waters based on relative chloride, sulphate and bicarbonate ions (Giggenbach 1991).

The thermal springs of Grn1, Grn, Olt3 and Eng2 Ndh, Arm and Ndl are characteristically considered to be diluted Cl-HCO_3/peripheral water that suffered considerable water-CO_2-rock interaction (e.g. Tian et al. 2018). These springs indicated the dilution of chloride fluids by either groundwater or bicarbonate water during lateral flow (e.g. Nicholson 1993). According to Nicholson (1993), the diluted Cl-HCO_3 waters are probably restricted to the margin of major up-flow zones and outflow structures of high-temperature systems. However, they are also discharged from springs in low-temperature systems and ELNB thermal water is a typical example.

Evaluation of mixing or dilution of thermal water

Chloride can serve as a useful tracer for geochemical cycling in hydrothermal systems because of its relatively conservative nature

(Wang et al. 2018). It is used in a linear relationship with other elements in the interpretation of the chemistry of thermal and cold waters and can be used to investigate the prevailing subsurface processes (Arnórsson 1985, Tian et al. 2018). The dissolved chemical constituents of thermal and cold water of LNB such as Na^+, HCO_3^-, Mg^{2+}, B^{3+}; and EC were correlated against Cl^- as shown in (Figure 5a-f).

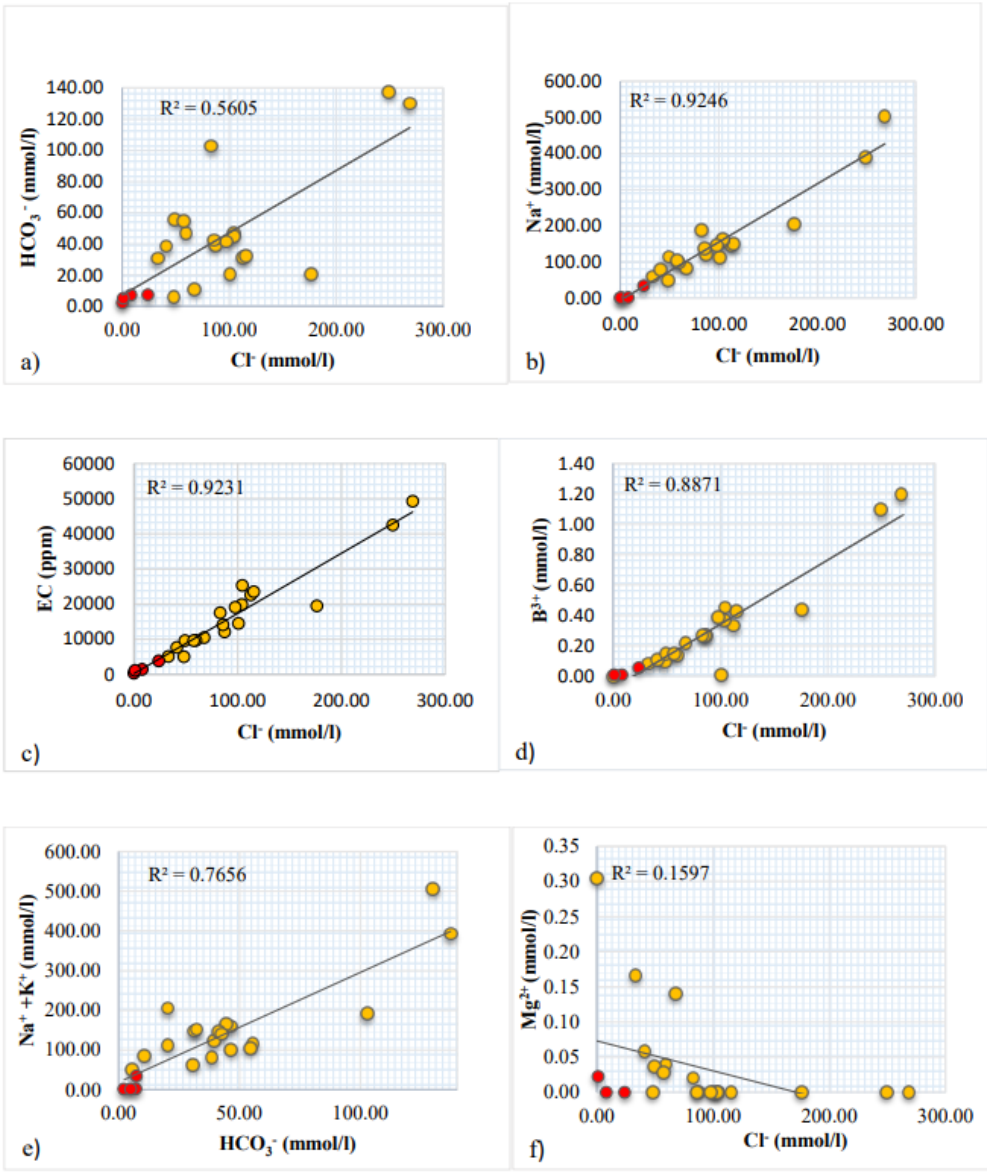

Figure 5: Relationships between various ions (EC, Na^+, K^+, Mg^{2+}, B^{3+}, HCO_3^- and Cl^-) for LNB thermal and cold water. R^2 denotes the coefficient of determination, red dots represent cold water and orange dots represent thermal water.

A high positive correlation was shown between Na^+ vs Cl^-, B^{3+} vs Cl^-; and EC vs Cl^- (R^2 = 0.88-0.96). The high correlation between Na^+ and Cl^- may be due to the

dilution of thermal water with the lake water that is highly evaporated, increasing the Cl^- content of the thermal water as shown by the water from Grn and Grn1. The prevalence of Na^+ against the rest of the cations could be attributed to the cation exchange processes between water and rocks leading to the formation of secondary minerals (Lambarkis et al. 2014). There is a high correlation between EC vs Cl^-, probably caused by a long interaction of water with host rocks, which have been affected by the re-dissolution and precipitation of brines in the basin. This may also suggest interactions of thermal water with the saline water from Lake Natron. An apparent mixing trend is also indicated by a positive correlation plot of B^{3+} vs Cl^-. A moderate correlation was shown between HCO_3^- vs Cl^- whereas no correlation is shown between Mg^{2+} vs Cl^-.

This moderate correlation may have resulted from the mixing of thermal water with the groundwater especially in the ELNB and in the south of WLNB (e.g D'Amor and Panichi 1985). The low correlation indicated by Mg^{2+} is due to the depletion of Mg^{2+} associated with the formation of Mg-rich secondary minerals within the hydrothermal system (Papachristou et al. 2014).

Conclusion

The geochemical analysis indicated that highly mineralised water is present in the LNB, with Na^+ being the major cation and Cl^- and HCO_3^- being the major anions. Three types of water were identified including Na-Cl water, Na-HCO_3 water and Ca-HCO_3 water. The Na-Cl water occurs in the thermal springs in both WLNB and ELNB. The thermal water in the west of the basin becomes progressively diluted towards the south due to the shallow groundwater incursion. In the ELNB, thermal waters had neutral to near neutral pH while Cl^- and HCO_3^- were more or less the same, thus both Na-Cl/Na-HCO_3 types of water were present. The geochemical evolution of water in the LNB, therefore, reflected the rocks' lithology and flow paths, as well as hydrothermal activities.

The Cl-SO_4-HCO_3 diagram categorised the LNB water into three classes featuring matured Cl water, mixed Cl-HCO_3/peripheral water and HCO_3 water. The HCO_3 water is water from shallow groundwater, rivers and cold springs. The mixed Cl-HCO_3/peripheral water is the water that has been affected by the dilution from other sources including rivers, the lake and shallow groundwater. Based on the correlation diagrams, it was concluded that the geochemical components of water such as chloride and sodium have a significant relationship, reflecting the processes that affect the water in the hydrothermal reservoir and on the surface, including ion exchange, dissolution, precipitation and mixing with rivers, lakes and groundwater.

The water-CO_2-Na/K-silicate interactions control the accumulation of components in the thermal water, forming the Na-HCO_3 water. Based on the hypothesised nature and observed geochemistry of thermal waters in the LNB, it is recommended to take precautions when planning geothermal projects because the high mineralisation of thermal water may cause corrosion and scaling of production facilities. Apart from that, there is a considerable mixing or dilution of thermal water with shallow groundwater which may affect the temperature and the composition of Cl^-.

Acknowledgements

This research was funded by the Tanzanian Ministry of Education Science and Technology under MoEST Scholarship.

References

Abdallah EA, Kasanzu CH, Kinabo CP, Imai A and Butler MJ 2022 Constraining the origin and age of the thermal and cold water in the Lake Natron Basin, northern Tanzania. *Tanz. J. Sci.* 48(4): 804-815.

Appelo CAJ and Postma D 2005 Geochemistry, groundwater and pollution, 2nd ed, Taylor & Francis Group PLC, NL.

Arnórsson S 1985 The use of mixing models and chemical geothermometers for estimating underground temperatures in

geothermal systems. *J. Volcanol. Geotherm. Res.* 23: 299-335.

Arnórsson S, Bjarnason JÖ, Giroud N, Gunnarsson I and Stefánsson A 2006 Sampling and analysis of geothermal fluids. *Geofluids* 6: 203-216.

D'Amore F and Panichi C 1985 Geochemistry in geothermal exploration. *Int. J. Energy Res*. 9: 277-298.

Davraz A 2014 Application of hydrogeochemical techniques in geothermal systems; examples from the eastern Mediterranean region. In: Baba A, Bundschuh J and Chandrasekaram D (Ed) *Geothermal systems and energy resources: Turkey and Greece*, Taylor and Francis Group, London, 7: 77-116.

Dawson JB 2008 The Gregory Rift Valley and Neogene-Recent volcanoes of Northern Tanzania. *Geol. Soc. Lond. Mem*. 33.

Eugster HP 1970 Chemistry and origin of the brines of Lake Magadi, Kenya. In: Morgan BA (Editor) *Fiftieth Anniversary Symposia: Mineralogy and petrology of the upper mantle sulfides; mineralogy and geochemistry of non-marine evaporites*: *Mineral. Soc. Am.* 3: 213-235.

Foster A, Ebinger C, Mbede E and Rex D 1997 Tectonic development of the northern Tanzanian sector of the East African Rift System. *J. Geol. Soc. Lond*. 154: 689-700.

Giggenbach WF 1988 Geothermal solute equilibria. Derivation of Na-K-Mg-Ca geoindicators. *Geochim. Cosmochim. Acta.* 52(12): 2749-2765.

Giggenbach WF 1991 Chemical techniques in geothermal exploration. In: D'Amore F (Coordinator), *Applied Geochemistry and Geothermal Resources Development*, UNITAR/UNDP publication, Rome. 119-142.

Guest NJ and Pickering R 1966a Brief explanation of the geology of Kibangaini. QDS028, *Geological Survey of Tanzania.*

Guest NJ and Pickering R 1966b Brief explanation of the geology of Gelai and Ketumbeine. QDS040, *Geological Survey of Tanzania*.

Guest NJ and Stevens JA 1951 *Lake Natron, its springs, rivers, brines and visible saline reserves.* Report (Nr.58) Geological Survey of Tanzania (pp.1-20).

Guest NJ, James TC, Pickering R and Dawson JB 1961 Brief explanation of the geology of Angata Salei. QDS039, *Geological Survey of Tanzania*.

Hochstein MP 1999 Geothermal systems along the East-African Rift. *Bull. d'Hydrogeol*. 17: 301-310.

Hochstein MP, Temu EP and Moshy CMA 2000 Geothermal resources of Tanzania. In: *Proceedings World Geothermal Congress, Kyushu-Tohoku*, 1233-1238.

Jones BF, Eugster HP and Rettig SL 1977 Hydrochemistry of Lake Magadi basin, Kenya. *Geochim. Cosmochim. Acta*. 41: 53-72.

Lambrakis N, Katsanou K and Siavalas G 2014 Geothermal fields and thermal waters of Greece: an overview In: Baba A, Bundschuh J and Chandrasekaram D (Ed) *Geothermal Systems and Energy Resources Turkey and Greece* vol. 7 (pp 25-42), Taylor and Francis Group, London.

Lee H, Fischer TP, Muirhead JD, Ebinger CJ, Kattenhorn SA, Sharp ZD, Kianji G, Takahata N and Sano Y 2017 Incipient rifting accompanied by the release of subcontinental lithospheric mantle volatiles in the Magadi and Natron basin, East Africa. *J. Volcanol. Geotherm. Res*. 346: 118-133.

Li C, Zhou X, Yan Y, Ouyang S and Liu F 2021 Hydrogeochemical characteristics of hot springs and their short-term seismic precursor anomalies along the Xiaojiang Fault Zone, Southeast Tibet Plateau. *Water* 13(19): 2638.

Mahecha A, Saadi N, Yonezu K, Watabane K and Mayalla J 2018 Mapping of hydrothermal alteration of the Lake Natron–Oldoinyo Lengai geothermal area in northern Tanzania using satellite imagery In: *Proceedings 7th African Rift Geothermal Conference, Kigali*.

Muirhead JD, Kattenhorn SA, Lee H, Mana S, Turrin BD, Fischer TP, Kianji G, Dindi E and Stamps DS 2016 Evolution of

upper crustal faulting assisted by magmatic volatile release during early-stage continental rift development in the East African Rift. *Geosphere* 12(6): 1670-1700.

Nicholson K 1993 Geothermal Fluids: geochemistry and exploration techniques. Springer-Verlag, Berlin Heidelberg.

Neukirchen F, Finkenbein T and Keller J 2010 The Lava sequence of the East African Rift escarpment in the Oldoinyo Lengai–Lake Natron sector, Tanzania. *J. Afr. Earth Sci.* 58(5): 734-751.

Papachristou M, Voudouris K, Karakatsanis S, D'Alessandro W and Kyriakopoulos K 2014 Geological setting, geothermal conditions and hydrochemistry of south and southeastern Aegean geothermal systems In: Baba A, Bundschuh J and Chandrasekaram D (Ed) *Geothermal Systems and Energy Resources Turkey and Greece.* Taylor and Francis Group, London, 7: 47-68.

Petrini R, Italiano F, Ponton M, Slejko FF, Aviani U and Zini L 2013 Geochemistry and isotope geochemistry of the Monfalcone thermal waters (northern Italy): inference on the deep geothermal reservoir. *Hydrogeol. J.* 21: 1275-1287.

Piper AM 1944 A Graphic procedure in the geochemical interpretation of water analyses. *Trans. Am. Geophys. Union* 25: 914-923.

Powell T and Cumming W 2010 Spreadsheets for geothermal water and gas geochemistry In: *Proceedings Thirty-Fifth Workshop on Geothermal Reservoir Engineering* Stanford University, Stanford, California. SGPT-TR-188: 1-10.

Tian J, Pang Z, Guo Qi, Wang Y, Li J, Huang T and Kong Y 2018 Geochemistry of geothermal fluids with implications on the sources of water and heat recharge to the Rekeng high-temperature geothermal system in the Eastern Himalayan Syntax. *Geothermics* 74: 92-105.

Wang X, Lu G and Hu BX 2018 Hydrogeochemical characteristics and geothermometry applications of thermal waters in coastal Xinzhou and Shenzao Geothermal Fields, Guangdong, China. *Geofluids* 2018: 8715080, 24 p.